JOURNAL OF GEOPHYSICAL RESEARCH, VOL. 104, NO. A5, PAGES 10,275–10,283, MAY 1, 1999

A study of the inner magnetosphere based on data of Polar

N. A. Tsyganenko,[1,2] G. Le,[3] C. T. Russell,[3] and T. Iyemori [4]

Abstract. A statistical study of the near-Earth equatorial magnetic field depression has been done on the basis of a set of data from 20 months of Polar magnetic field experiment in 1996–1997, supported by simultaneous information on the solar wind state by Wind and IMP 8 spacecraft. This work addresses the spatial distribution of the magnetic field, produced by magnetospheric currents near the dipole equator at radial distances between 2.0 and 4.5 R_E, and its dependence on the ground Dst field, solar wind pressure, and interplanetary magnetic field (IMF). The observed radial and local time variation of the regression coefficients in the expansion for the disturbance field is interpreted in terms of the relative contribution of the principal magnetospheric currents. The inner field has a significant noon-midnight and dawn-dusk asymmetry, sensitive to Dst and to the solar wind pressure. The results confirm the high quality of the Polar magnetic field experiment (MFE) data in a wide range of altitudes and will be a useful guide for the modeling of the inner magnetosphere.

1. Introduction

Accurate modeling of the near-Earth magnetic environment is of central importance for the physics of Sun-Earth connections, since the geomagnetic field underlies basic processes in the geospace plasma and links the interplanetary medium with the ionosphere and upper atmosphere. The magnetic field in the inner magnetosphere is especially interesting from the viewpoint of the space weather prediction, since the region earthward of the synchronous orbit is populated by many commercially important satellites (e.g., Global Positioning System), whose radiation environment is closely tied to the dynamics of the geomagnetic field there.

One central problem in the data-based modeling of the magnetosphere is the choice of input parameters, quantifying the contributions from individual electric current systems to the total field. In order to allow the reconstruction and short-term forecasting of dynamically varying geomagnetic configurations, these parameters should include the characteristics of the solar wind, routinely monitored at a sufficiently high time resolution. The accuracy of inner magnetospheric field models can be greatly improved by using high-resolution ground-based magnetic data, in particular, the new longitudinally symmetric (SYM) and asymmetric (ASY) indices by *Iyemori* [1990], an extension of the standard Dst index. Combined with data on the solar wind state, those indices can provide valuable information on the strength and distribution of the electric current in the near-Earth space.

This work addresses the structure of magnetic field of external sources in the inner equatorial region ($2.2 \leq R \leq 4.5 R_E$), as observed by the Polar spacecraft. Although the orbit of Polar was designed primarily for studying the high-latitude magnetosphere, the spacecraft also probed a relatively wide interval of radial distance at low magnetic latitudes, owing to the seasonal rotation of the orbit plane in the GSE coordinates and owing to the diurnal wobbling of the Earth's dipole axis. Thanks to the high precision of the determination of spacecraft attitude, the Polar magnetometer was found to provide quite accurate values of the external field even near perigee, as was demonstrated recently by *Le and Russell* [1998] in their study of the magnetic field over the polar cap. In contrast to the analysis of Le and Russell, this work addresses the disturbance field at low solar magnetic latitudes.

Previous studies of this region included the first statistical mapping in the magnetosphere of the scalar difference ΔB between the total observed field magnitude and a reference field due to the Earth's internal sources [*Sugiura et al.*, 1971]. That work was based on rubidium magnetometer data taken by OGO-3 and OGO-5 spacecraft, and it provided evidence of a significant dawn-dusk and noon-midnight asymmetry of the ΔB contours. However, the data were binned into just two intervals of the Kp index, and no attempt was made to quantitatively relate the disturbance field with solar wind conditions and/or with the Dst index.

Fairfield et al. [1987] conducted another statistical study of the near-Earth equatorial field using Active Magnetospheric Particle Tracer Explorers (AMPTE)/CCE data. However, only the midnight region was addressed in that work, and again, no parameterization of the observed field was made, except for binning it into a few intervals of the Kp index.

[1]Extraterrestrial Science Department, Raytheon ITSS Corporation, Lanham, Maryland.

[2]Also at Laboratory for Extraterrestrial Physics, NASA Goddard Space Flight Center, Greenbelt, Maryland.

[3]Institute of Geophysics, University of California, Los Angeles.

[4]Data Analysis Center for Geomagnetism and Space Magnetism, Kyoto University, Kyoto.

Paper number 1998JA900160.
0148-0227/99/1998JA900160$09.00

Iijima et al. [1990] analyzed the local time structure of the equatorial magnetic field on the basis of 180 days of AMPTE/CCE data, acquired in 1985 and 1986. Their data set covered prolonged periods of severely disturbed conditions; however, no attempt was made to quantify the dependence of the average local disturbance field on the *Dst* index or the solar wind state.

The present work concentrates on the noon-midnight and dawn-dusk distributions of the magnetic field from external sources in the near-Earth equatorial region and on its dependence on the solar wind pressure, the symmetrical part (SYM-H) of the *Dst* field (for brevity, referred henceforth as *Dst*), and on the interplanetary magnetic field (IMF). Accordingly, the study used three data sets, covering the 20-month period between March 20, 1996, and November 30, 1997: (1) the solar wind and IMF data taken by IMP 8 and Wind, (2) the 5-min average *Dst*, and (3) the magnetospheric magnetic field data of Polar. Section 2 addresses those data in more detail; a numerical procedure of the data analysis is described in section 3, followed by a discussion of the results in section 4 and by a summary of our findings in section 5.

2. Data Description

2.1. Solar Wind Data

This study used 5-min averaged solar wind and IMF data, compiled from the higher-resolution data of two monitoring spacecraft: IMP 8 and Wind. The IMP 8 solar wind plasma data were created from 1-min averages, provided by the Massachusetts (MIT) website, while the IMF data were calculated from 15-s averages, retrieved from the National Space Science Data Center (NSSDC) on-line database. Both the solar wind and IMF data of the Wind spacecraft were obtained from the NSSDC website with 1-min resolution and were subsequently averaged over 5-min intervals.

In order to minimize possible contamination of the solar wind data by measurements made in the magnetosheath, a selection of the data points was made using an average bow shock model of *Peredo et al.* [1995], and an upper limit was imposed on the deflection of the flow from the antisunward direction, by requiring that $(V_Y^2 + V_Z^2)^{1/2} \leq 0.15|V_X|$. An additional constraint was also imposed on the Wind data, leaving out points with $(Y^2 + Z^2)^{1/2} \leq 40R_E$, as being too far from the Sun-Earth line. The original data also contained a small percentage of isolated records with abnormally high density ($N > 50$ cm^{-3}) or with unrealistically large spikes of IMF. Such suspicious records were visually checked and deleted.

To take into account the finite travel time of the solar wind from the upstream location of the monitoring spacecraft, observation times for all the data were reduced to the Earth's location by introducing a time shift $\tau = X/|V_X|$, where X and V_X are the spacecraft position on the Sun-Earth line and the flow velocity component parallel to that line, respectively. When both Wind and IMP 8 data were available for a given 5-min interval and when both satisfied the above requirements, then IMP 8 data records were preferred, since most Wind measurements were made at much larger upstream distances and hence could have contained larger errors.

The mixing of the data from two different spacecraft at widely separated locations raises the interesting question of their compatibility, discussed lately in several works [e.g., *Paularena et al.*, 1998]. In order to quantitatively assess possible inaccuracies, resulting from the extrapolation of more distant Wind measurements to the vicinity of Earth, we studied correlations between the 5-min average data of Wind and IMP 8 over the 3-year period 1995–1997. An intersection of the Wind and IMP 8 data sets was created for that period, i.e., a set of IMF and plasma parameters, measured by the two spacecraft and corresponding to the same arrival time of the solar wind to the plane $X_{GSE} = 0$ (based on observed values of V_x). In this test study, more severe restrictions were imposed on the positions of both spacecraft; namely, we required that $\rho = \sqrt{Y^2 + Z^2} < 20\,R_E$ and $X_{GSE} > 20\,R_E$. The resultant intersection set included a total of 5832 records.

Correlation coefficients for the IMF B_x, B_y, and B_z were found equal to 0.94, 0.96, and 0.89, respectively, with slopes very close to unity (1.00, 1.01, and 1.01, respectively). For the Sun-Earth component of the flow velocity, V_x, the correlation coefficient was found 0.99, while the density N and thermal velocity V_{th} yielded 0.97 and 0.89, respectively. The slopes for V_x and V_{th} were quite close to unity (1.02 and 1.00, respectively); however, the proton density yielded the slope 0.88, indicating a possible $\sim$ 10% overestimate by the IMP 8 instrument. A more detailed study of that discrepancy is planned for the future by the MIT group, though we do not expect it to significantly affect the results of the present study, owing to a relatively low share of IMP 8 data in the solar wind data base (34% for 1996 subset and 25% for 1997).

Scatter plots of the above quantities are shown in Figure 1. Overall, the results confirm a good quality of the distant Wind data and suggest using them in combination with the IMP 8 data, after proper filtering and after editing out of bad records.

2.2. Polar Magnetic Field Data

The orbit of Polar and the magnetic field experiment (MFE) on board the spacecraft was described in detail elsewhere [e.g., *Le and Russell*, 1998, and references therein] and will not be addressed here. The first step in processing the original data of the Polar MFE was to tag the observed field vectors (1-min averages) by the solar wind data and by 5-min average values of the *Dst* field, obtained from the symmetrical part (SYM-H) of the new 1-min index by *Iyemori* [1990]. Then an automated search was made for suspicious records with erroneous values of the spacecraft ephemeris (accompanied by abnormal jumps in the field components). All such records were visually checked and eliminated. The percentage of the bad records significantly increased near the perigee segments of the Polar orbits, which is why we imposed a lower limit $R_{min} = 2.2\,R_E$ upon the radial distance. We also required that each data record of Polar be accompanied by solar wind information; owing to the availability of data from two solar wind monitoring spacecraft, the total percentage of solar wind data gaps was relatively low. A visual inspection of all the data was made by plotting observed values of the external field (i.e., total observed $\vec{\mathbf{B}}$ minus International Geomagnetic Reference Field (IGRF)) along with those predicted by the T96_01 version of the data-based model [*Tsyganenko*, 1995, 1996], using the concurrent values of the solar wind parameters and of the *Dst* field. This procedure was quite helpful in identifying erroneous spikes in the solar wind pressure

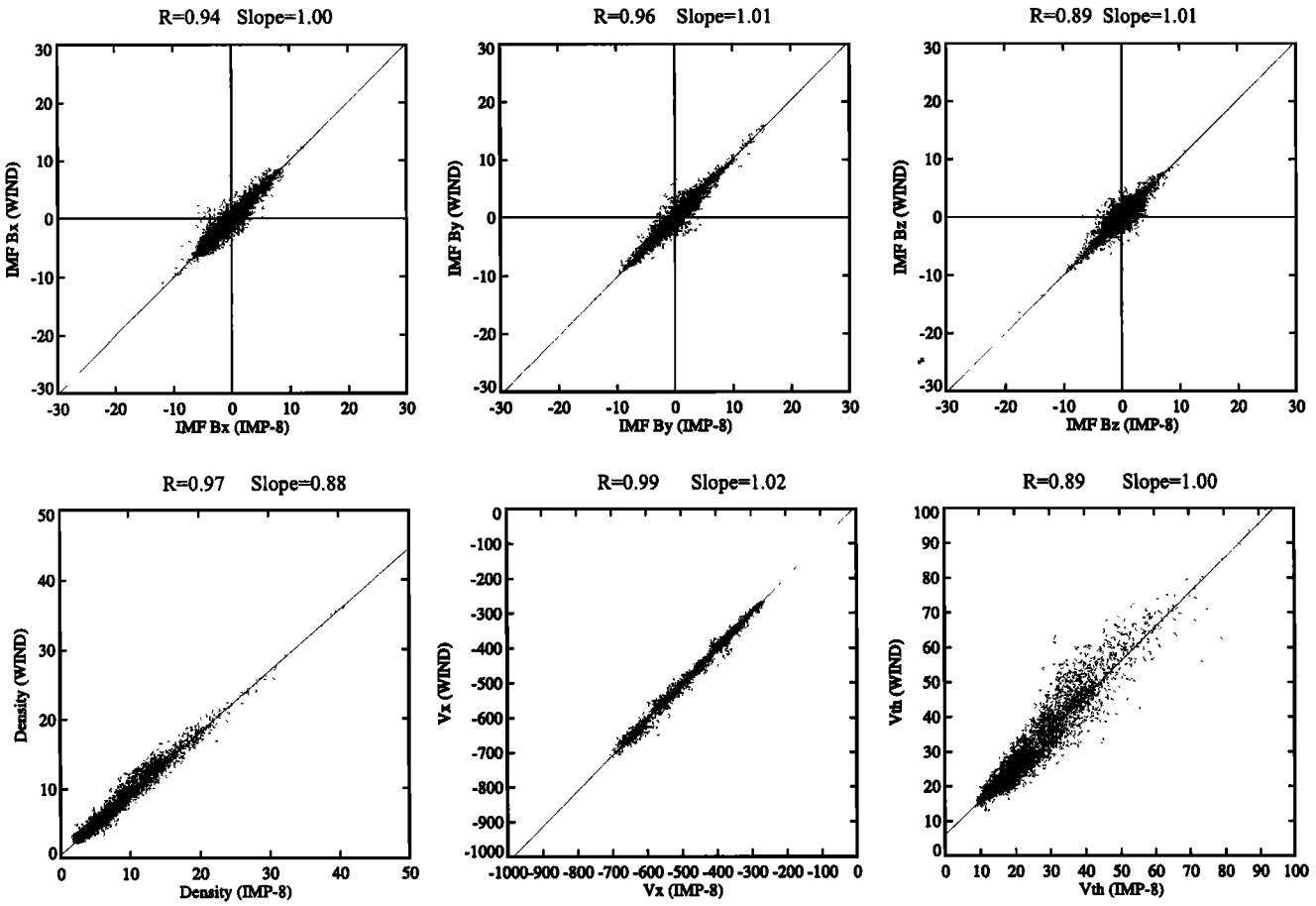

Figure 1. Scatter distributions of (top) three components of the interplanetary magnetic field (IMF) in nanotesla and (bottom) solar wind parameters, proton density in cm^{-3}, bulk velocity V_x, and thermal speed V_{th} in km s^{-1}. The IMF and solar wind parameters were measured by Wind and plotted against the same quantities, observed simultaneously by IMP 8 during the period 1995-1997. The data points correspond to 5-min averaged parameters; the time lag has been taken into account owing to the finite travel time of the solar wind between both spacecraft and Earth.

and IMF, overlooked in the earlier processing of the solar wind data. Figure 2 shows a sample of the daily plot of the field components observed by Polar, along with those given by the model. After the visual inspection the data were averaged over 5-min intervals. The final data set included 123,753 records, covering the period from March 20, 1996, to November 30, 1997.

3. Data Analysis

This work concentrates on the structure of the low-latitude inner magnetosphere, as probed by Polar in the vicinity of the dipolar equator. For that reason, no attempt was made to model the total vector field. Instead, only the north-south component of the disturbance field was analyzed, since the external sources contribute mainly to B_{ZSM} in that region.

The data of Polar from the set, described in section 2, were binned into four sectors of the solar-magnetic longitude, each 70° in width and centered on noon, dusk, midnight, and dawn, and (for each of the four longitude sectors) five equal bins of the distance $\rho = \sqrt{X_{SM}^2 + Y_{SM}^2}$ within the interval $2.0 \le \rho \le 4.5\ R_E$. In this study we did not attempt to comprehensively model the inner magnetosphere; the primary goal was to investigate its noon-midnight and dawn-dusk structure. For that reason the data covered only $\approx 82\%$ of the entire range of the longitude, and the solar-magnetic latitude of the observations was limited to a narrow interval of ±12° around the dipole equator. An additional limitation on the data was a requirement that the values of Dst lie within the range $-40 \le Dst \le 0$. That restriction was intended to approximately equalize the average values of the Dst field for all bins and thus to eliminate possible spurious effects due to different average disturbance levels of individual data bins (we thank one of the referees for pointing out that possibility.) The binning yielded $4 \times 5 = 20$ subsets; the numbers of the data points in them are given in Tables 1–4.

For each subset the disturbance field was fitted to a linear function

$$B_{ZSM} = B_0 + B_1\left(Dst - \langle Dst\rangle\right) + B_2\left(\sqrt{P_{dyn}} - \sqrt{\langle P_{dyn}\rangle}\right) + B_3\left(\chi - \langle\chi\rangle\right) \quad (1)$$

of the Dst index, the square root of the solar wind dynamic pressure P_{dyn}, and the IMF-dependent quantity χ =

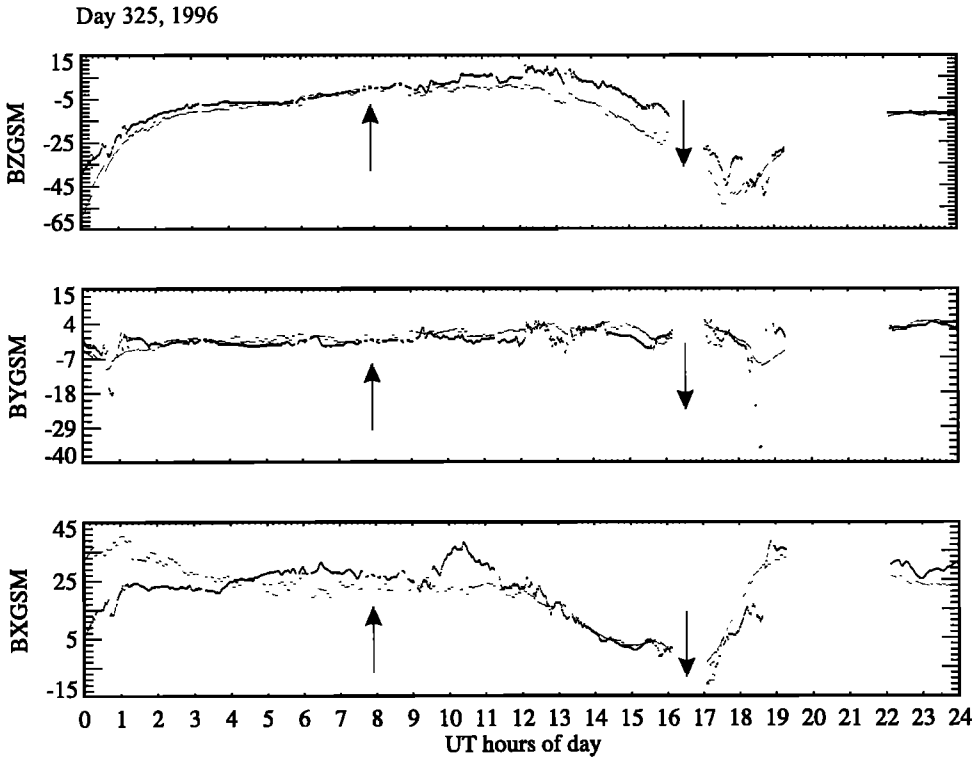

Figure 2. A sample plot of the variation of three GSM components of the magnetic field as observed by Polar (thick line) and that predicted by the data-based model (thin line) for the day of November 24, 1996 (Day 325). Note that the International Geomagnetic Reference Field (IGRF) has been subtracted from the Polar data and that it has not been included in the model field. In other words, the plots correspond to the external part of the total field only. Upward and downward arrows indicate the apogee and perigee times, respectively.

$B_t \sin(\theta/2)$, where $B_t = \sqrt{B_y^2 + B_z^2}$ is the IMF transverse component and θ is the IMF clock angle; the angular brackets denote averaging over the subsets. Our approach was to find best fit values of the coefficients in (1) for each subset, in order to determine the radial and local-time distribution of the disturbance field and its response to the solar wind state and to the Dst field. Note that the last term in (1) is a function of the IMF components only: to minimize possible intercorrelation between the coefficients B_3 and B_2, we intentionally did not include any of the solar wind plasma parameters in that term (as, for example, in the widely used solar wind magnetosphere coupling parameter $\epsilon = V B_t^2 \sin^4(\theta/2)$). Likewise, we did not try to experiment with different possible forms of χ (e.g., by assuming various powers of B_t and $\sin(\theta/2)$): most of the IMF effects are already indirectly present in the Dst field, and this is why the relative importance of the last term in (1) was found to be quite small, as discussed in more detail in section 4.

The values of the coefficients B_0–B_3 were fitted to the data in each of the 20 subsets, using a standard linear least squares technique. Figure 3 displays 20 scatterplots of the observed B_{ZSM} versus its approximation by (1). In each plot, the correlation coefficient R between data and model is indicated, ranging between 0.50 and 0.85.

Tables 1–4 display the results of the calculation for four sectors of solar-magnetic longitude (noon, dusk, midnight, and dawn, respectively). Five columns in each of the tables correspond to five intervals of the radial distance ρ and contain average values of Dst, P_{dyn}, and χ, followed by the best fit values of the coefficients B_0–B_3. The numbers N of the data points (first row) in most bins lie between 100 and 400; the largest one (488) occurred in the midnight bin with $3.0 \leq \rho < 3.5$, while the smallest number (22) was found in the dusk bin with $2.0 \leq \rho < 2.5$. The values of the coefficients are provided with corresponding uncertainties, assuming a normal distribution of sample values around their mean values [e.g., *Bevington*, 1992]. As can be seen from Tables 1–4, even for bins with relatively small numbers of data points, the errors remain tolerably small.

Using the tables, one can calculate from (1) the disturbance field in each of the longitude-distance bins, for any combination of the solar wind parameters and Dst. In section 4 we discuss the obtained results in more detail.

4. Discussion

Using the values of the coefficients B_0–B_3 from Tables 1–4, we plotted them in Figure 4 as functions of the position on the noon-midnight (X_{SM}) and dawn-dusk (Y_{SM}) axes. The horizontal widths of the shaded rectangles indicate the range of radial distances in each bin, while their heights show the estimated statistical error of the coefficients. Each of the plots has a gap in the middle, because we excluded the near-perigee data from the analysis.

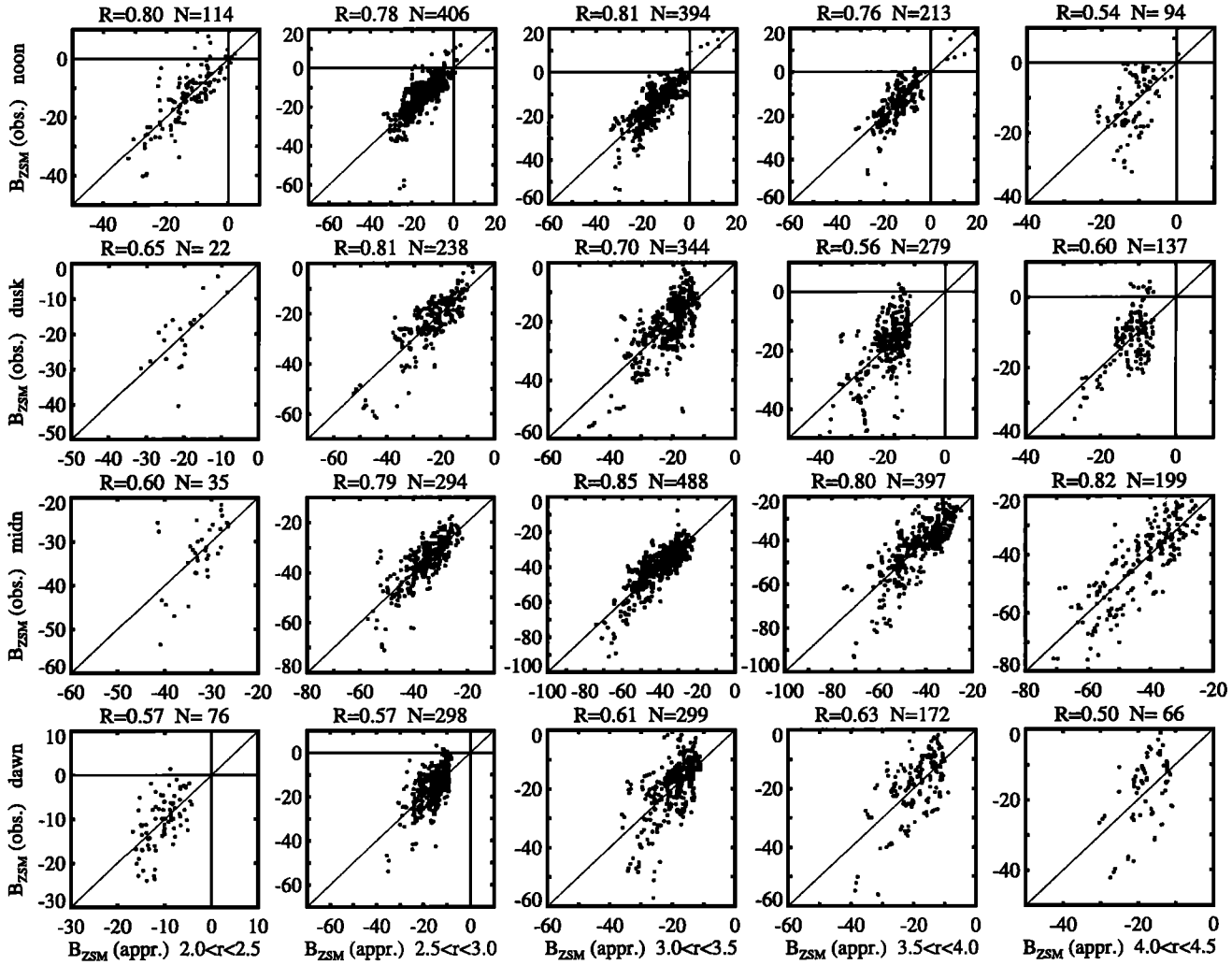

Figure 3. Scatterplots of the observed B_{ZSM} component of the magnetic field, produced by external magnetospheric sources, against the values obtained from equation (1), using the corresponding values of Dst, P_{dyn}, and IMF components. The 20 plots correspond to four sectors of the magnetic local time and five bins of the radial distance, as is indicated on the left side and bottom of Figure 3.

The constant term B_0 corresponds to the average disturbance B_{ZSM}, expected to be observed when Dst, P_{dyn}, and χ are equal to their average values. As can be seen in Figure 4 (first column from left), the average disturbance is negative in the entire range of distances under study, reaching its most negative values in the midnight sector at $X_{SM} \sim -4$, where the contributions from the ring current and the near-earth tail current are the strongest. In the noon sector the disturbance field is higher by ~ 30 nT than that at midnight, owing to a weaker contribution of the nightside currents and because of a much stronger effect of the dayside magnetopause currents. This is quite close to what one could expect on the basis of earlier observations and models.

The dawn-dusk profile of B_0 reveals a significant asymmetry. Although the difference in the magnitudes of the dawn and dusk minima is just $\sim 15\%$, the dusk minimum is located at $Y_{SM} \sim 2.8\ R_E$, while on the dawnside it appears at $Y_{SM} \sim 3.3\ R_E$. This implies a deeper penetration of the equatorial currents onto inner L-shells in the dusk magnetosphere than that at dawn, even under average conditions.

The coefficient B_1 (second pair of panels from left in Figure 4) quantifies the dependence of the disturbance field on Dst. As can be seen in Figure 4 (top), the response of the field to Dst decreases sunward, from $B_1 = 1.12$ at $X_{SM} = -4.25$ to $B_1 = 0.28$ at $X_{SM} = 4.25$. A simple interpretation of that feature is as follows. The symmetric part of the Dst field, entering in (1), is a sum of (1) the Chapman-Ferraro field from the magnetopause currents, proportional to $\sqrt{P_{dyn}}$ and (2) the field B_e produced by other external sources, mostly by the ring current and, to a lesser extent, by the near-Earth part of the tail current sheet. More specifically,

$$Dst = a_0 + a_1\sqrt{P_{dyn}} + a_2\, B_e \qquad (2)$$

where the additive constant a_0 depends on the definition of the baseline, the coefficient a_1 (on the order of 10–15) can be estimated from the pressure balance equation, combined with a realistic model of the magnetopause shielding field [e.g., *Russell et al.*, 1994a, b; *Tsyganenko*, 1996], and the coefficient a_2 is a correction factor in the range 1.2–1.4, depending

Table 1. Results of the Fitting of Equation (1) to the Data of Polar, Taken in the Noon Sector of the Equatorial Magnetosphere, for Five Intervals of the Radial Distance ρ

	$2.2<\rho<2.5$	$2.5<\rho<3.0$	$3.0<\rho<3.5$	$3.5<\rho<4.0$	$4.0<\rho<4.5$
		Data Set Characteristics			
N	114	406	394	213	94
$\langle Dst \rangle$	-14.20	-14.22	-14.32	-13.86	-16.17
$\langle P_{dyn} \rangle$	2.55	2.45	2.47	2.53	2.61
$\langle \chi \rangle$	2.43	2.64	2.57	2.45	2.07
		Best Fit Coefficients			
B_0	-12.7±0.6	-13.9±0.3	-13.8±0.3	-13.3±0.4	-10.7±0.7
B_1	0.71±0.07	0.67±0.04	0.62±0.03	0.54±0.05	0.28±0.10
B_2	8.1±1.5	8.7±0.9	11.0±0.8	10.8±1.3	15.8±2.9
B_3	-0.80±0.34	-0.86±0.17	-0.46±0.14	0.43±0.17	-0.9±0.7

on the assumed model of the Earth's conductivity and on the scale of the time variation of the disturbance field.

Consider a "partial" variation δB_e of the field at Earth's surface, that is, assuming no change in the magnetopause currents. In this case, from (2), $\delta Dst = a_2 \delta B_e$, and hence, from (1), $\delta B_{ZSM} = B_1 a_2 \delta B_e$, which means that $B_1 a_2$ can be viewed as a coefficient of proportionality between the variation of B_{ZSM} at a particular location in the equatorial magnetosphere and the concurrent variation of the disturbance field at the Earth's location, caused by a change in the strength of the ring/tail currents. Therefore the profiles of B_1 against X_{SM} and Y_{SM} in Figure 4 provide the spatial distribution of the incremental disturbance from the magnetospheric sources per 1 nT variation of the Dst, assuming a fixed magnetopause field. This naturally explains the obtained decrease of B_1 in the sunward direction and can be concisely formulated as follows: most of the intramagnetospheric sources contributing to the Dst reside on the nightside. Indeed on the basis of AMPTE/CCE data, *Iijima et al.* [1990] reported a strong noon-midnight asymmetry of the electric current in the inner magnetosphere ($\rho \leq 8.8\ R_E$), with the nightside current being 2–3 times larger than that on the dayside.

Turning to the dawn-dusk profile of B_1 (Figure 4, bottom; second column from the left), we again observe a significant asymmetry. Whereas in the outer bins ($\rho \geq 3.0$) the dawn and dusk values of B_1 are nearly equal, their radial variation in the inner region is different: on the dawnside, B_1 peaks at $\rho \approx 3.5$ and then rapidly decreases earthward, while on the duskside it peaks at a closer distance and reaches there significantly larger values. This means that variations of the Dst field due to the magnetospheric sources are accompanied by strongly asymmetric disturbances in the innermost magnetosphere, so that the largest contribution to Dst comes from the dusk currents, in agreement with earlier findings [e.g., *Cahill*, 1966; *Crooker and Siscoe*, 1981].

The third column in Figure 4 displays the spatial distribution of the effects of the solar wind pressure changes. In this case, again, one can see strong asymmetries, both in the noon-midnight direction and in the dawn-dusk direction. The coefficient B_2 is negative on the nightside and rapidly grows sunward, reaching its largest positive values at the location closest to the subsolar magnetopause. Again, this is what one should expect, based on simple physics: on the nightside an increase in P_{dyn} results in a compression of the tail lobes, hence, in a stronger cross-tail current, leading to a deepening of the B_{ZSM} depression. On the dayside, the northward field of the subsolar magnetopause currents becomes a dominant factor, which results in the opposite response of the B_{ZSM} to the the pressure variations. The dawn-dusk profile of the coefficient B_2 (Figure 4, bottom) is also strongly asymmet-

Table 2. Results of the Fitting of Equation (1) to the Data of Polar, Taken in the Dusk Sector of the Equatorial Magnetosphere, for Five Intervals of the Radial Distance ρ

	$2.2<\rho<2.5$	$2.5<\rho<3.0$	$3.0<\rho<3.5$	$3.5<\rho<4.0$	$4.0<\rho<4.5$
		Data Set Characteristics			
N	22	238	344	279	137
$\langle Dst \rangle$	-9.62	-11.32	-9.97	-9.37	-8.12
$\langle P_{dyn} \rangle$	2.24	2.20	2.21	2.26	2.28
$\langle \chi \rangle$	2.08	2.52	2.33	2.25	2.10
		Best Fit Coefficients			
B_0	-20.3±1.5	-23.3±0.4	-21.8±0.4	-18.5±0.5	-11.8±0.5
B_1	0.87±0.25	0.95±0.05	0.77±0.05	0.75±0.07	0.67±0.09
B_2	3.4±5.0	2.5±1.4	-1.5±1.3	-1.4±1.7	2.0±2.4
B_3	-2.1±1.2	-1.5±0.2	-1.0±0.3	-0.2±0.3	-0.2±0.4

Table 3. Results of the Fitting of Equation (1) to the Data of Polar, Taken in the Midnight Sector of the Equatorial Magnetosphere, for Five Intervals of the Radial Distance ρ

	$2.2<\rho<2.5$	$2.5<\rho<3.0$	$3.0<\rho<3.5$	$3.5<\rho<4.0$	$4.0<\rho<4.5$
		Data Set Characteristics			
N	35	294	488	397	199
$\langle Dst \rangle$	-16.99	-14.37	-14.82	-14.25	-13.46
$\langle P_{dyn} \rangle$	2.28	2.31	2.27	2.33	2.36
$\langle \chi \rangle$	2.59	2.42	2.65	2.60	2.53
		Best Fit Coefficients			
B_0	-32.4±1.1	-35.8±0.3	-40.2±0.3	-42.7±0.4	-42.5±0.5
B_1	0.38±0.13	0.74±0.04	0.92±0.03	0.98±0.05	1.12±0.06
B_2	-5.8±4.1	-7.5±1.1	-12.5±1.0	-10.4±1.3	-11.9±2.0
B_3	-0.6±0.8	-1.1±0.2	-1.2±0.1	-1.7±0.2	-1.9±0.3

ric: there is just a minor response of B_{ZSM} to the pressure on the duskside, while on the dawnside we observe a dramatic variation of that response with ρ. The effect has opposite signs at small and large distances: while B_{ZSM} grows with P_{dyn} near Earth, in the outer bins the field depression deepens markedly. A possible interpretation is the dawn-dusk asymmetry in the radial profiles of the electric current: in the dawn sector the maximum of the current is located farther from Earth, and hence its increase results in a decrease of B_{ZSM} near the inner edge of the current, while at closer distances the northward field of the magnetopause current prevails. On the duskside the maximum of the current extends much closer to Earth, and hence its pressure-related increase results in a much smaller variation of B_{ZSM}, which is entirely offset by a positive contribution from the magnetopause current.

Finally, as can be seen from Tables 1–4 and in the fourth column Figure 4, the coefficient B_3 is close to zero in the noon and dawn sectors, while on the nightside and for $\rho < 3$ at dusk, it becomes significant and negative. Most likely, this reflects an enhancement of the depression due to the storm-time particle injections during the periods with large southward IMF B_z (and, hence, large positive χ in (1)). The relatively small regression coefficients for χ are due, first, to a delayed response of the ring current to the IMF-related magnetospheric effects and, second, to the fact that most of that response is already indirectly taken into account by the second term in (1), i.e., via the Dst field.

It is interesting to compare the disturbance field given by (1) with that obtained by *Iijima et al.* [1990] from AMPTE/CCE data. The bottom panel of Figure 1 of Iijima et al. gives a plot of the local-time distribution of ΔB_z (essentially the same quantity as our B_{ZSM} given by (1)) for $L = 4\,R_E$. No information on the average solar wind conditions was given by Iijima et al., but they did provide the average Dst for their data set, equal to -34 nT. Assuming $P_{dyn} = \langle P_{dyn} \rangle$, $\chi = \langle \chi \rangle$, and using the arithmetic mean values of the parameters for the bins $3.5 < \rho < 4.0$ and $4.0 < \rho < 4.5$ from Tables 1–4, we obtain for B_{ZSM} at noon, dusk, midnight, and dawn, the values -20.0, -33.2, -64.0, and -34 nT, respectively. The corresponding average values for the 70° local time sectors, centered at the same local times, from the plot of *Iijima et al.* [1990] equal approximately -27, -57, -71, and -36 nT, respectively. The largest difference is found in the dusk values: our data predict almost equal disturbance field at $\rho = 4\,R_E$ both at dawn and dusk, while according to Iijima et al., the dusk field depression is ~ 20 nT deeper than that at dawn. The most plausible explanation for that discrepancy is the difference in the range of the Dst values: in our study it is between -40 and 0, with $\langle Dst \rangle \sim -10$, while Iijima et al. used much more disturbed data with $-70 \le Dst \le -20$ and $\langle Dst \rangle \sim -34$. A further

Table 4. Results of the Fitting of Equation (1) to the Data of Polar, Taken in the Dawn Sector of the Equatorial Magnetosphere, for Five Intervals of the Radial Distance ρ

	$2.2<\rho<2.5$	$2.5<\rho<3.0$	$3.0<\rho<3.5$	$3.5<\rho<4.0$	$4.0<\rho<4.5$
		Data Set Characteristics			
N	76	298	299	172	66
$\langle Dst \rangle$	-9.74	-11.35	-11.37	-11.06	-10.16
$\langle P_{dyn} \rangle$	2.21	2.24	2.15	2.07	1.94
$\langle \chi \rangle$	2.33	2.38	2.20	2.24	2.17
		Best Fit Coefficients			
B_0	-10.3±0.6	-16.8±0.4	-19.8±0.4	-19.1±0.6	-18.1±1.1
B_1	0.4±0.1	0.61±0.06	0.72±0.06	0.72±0.08	0.57±0.14
B_2	9.6±2.5	3.7±1.7	-2.7±1.5	-8.7±2.3	-8.4±4.2
B_3	-0.11±0.40	-0.64±0.30	-0.11±0.30	-0.3±0.5	0.0±0.7

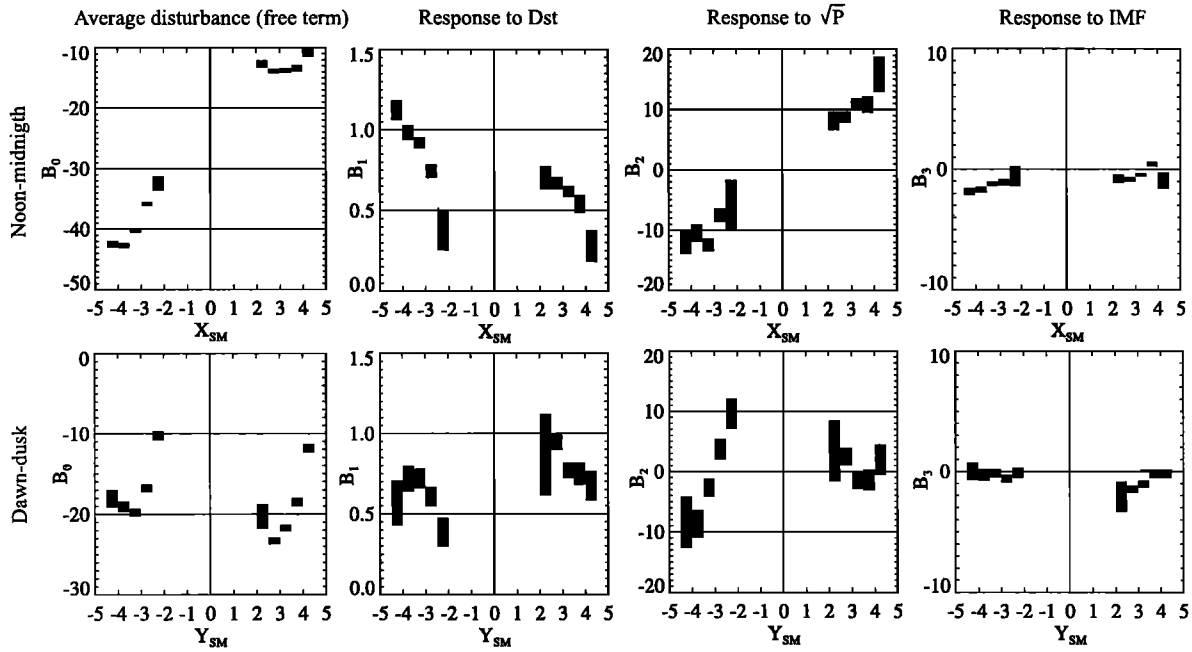

Figure 4. Variation of the regression coefficients of equation (1) in the solar magnetic equatorial plane along the (top) noon-midnight and (bottom) dawn-dusk directions. The centers of the shaded bars indicate the obtained values of the coefficients, their horizontal widths correspond to the size of the radial bins, and their heights show statistical uncertainties.

study of that question is planned, based on much larger data sets and more sophisticated magnetic field representations.

5. Conclusions

We have studied the spatial structure of the inner equatorial magnetospheric field depression and its dependence on *Dst* and on the solar wind and IMF parameters, on the basis of 20 months of data of Polar magnetic field experiment and on concurrent measurements in the interplanetary medium by IMP 8 and Wind. The magnetic field data in the range of radial distances between $\rho = 2.2$ and $4.5\ R_E$ were binned into five intervals of ρ and into four local-time sectors, and they were fitted to a linear regression form, representing the response of the north-south component B_{ZSM} of the field of external magnetospheric sources to *Dst*, $P_{dyn}^{1/2}$, and to the IMF-dependent parameter χ. The obtained best fit relationship will be useful for checking and parameterizing quantitative models of the near-Earth magnetic field.

The average values of B_{ZSM} were found to have a pronounced asymmetry, with much deeper field depression on the nightside as compared with the dayside, in agreement with existing models and earlier observations. The average depression is also asymmetric in the dawn-dusk direction, with the dusk minimum being observed significantly closer to Earth than in the dawn sector.

A significant spatial asymmetry was also found in the response of the disturbance field B_{ZSM} to *Dst*. That response is maximal on the nightside and rapidly falls off sunward, indicating that the most contribution to *Dst* on Earth comes from the nightside magnetospheric current. The dawn-dusk profile of the response of B_{ZSM} to *Dst* is also strongly asymmetric, which can be interpreted as a result of predominance of the contribution from duskside sources in the observed variations of the *Dst* field.

The effect of the solar wind pressure changes is also asymmetric, both in the noon-midnight direction and in the dawn-dusk direction, which can again be explained in terms of the combined effects of P_{dyn} upon the major sources of the external field. Finally, the direct contribution from the IMF-related term was found to be relatively weak, probably, in part, because the IMF effects are already indirectly present in the variation of the *Dst* field.

Acknowledgments. We wish to thank the IMP 8 and Wind Magnetometer Data Processing Teams for the IMF data of those spacecraft, K. Ogilvie for providing the solar wind data of Wind, and A. Lazarus for providing the solar wind data of IMP 8. The data were retrieved using the NSSDC on-line facilities (SPYCAT and CDAWEB). We are also grateful to the Referee 1 for pointing out the possibility of spurious effects due to the difference in the average values of *Dst* for individual subsets, and to David Stern for his careful reading of and many comments on the manuscript. This work is supported by NASA grant NASW-97024 (ISTP GI Program) and NSF Magnetospheric Physics Program grant ATM-9501463.

Hiroshi Matsumoto thanks S. Kokubun and T. J. Pulkkinen for their assistance in evaluating this paper.

References

Bevington, P. R., and D. K. Robinson, *Data Reduction and Error Analysis for the Physical Sciences,* McGraw-Hill, New York, 1992.

Cahill, L. J., Jr., Inflation of the inner magnetosphere during a magnetic storm, *J. Geophys. Res., 71,* 4505, 1966.

Crooker, N. U., and G. L. Siscoe, Birkeland currents as the cause

of the low-latitude asymmetric disturbance field, *J. Geophys. Res., 86*, 11,201, 1981.

Fairfield, D. H., M. H. Acuna, L. J. Zanetti, and T. A. Potemra, The magnetic field of the equatorial magnetotail: AMPTE/CCE observations at $R < 8.8 R_E$, *J. Geophys. Res., 92*, 7432, 1987.

Iijima, T., T. A. Potemra, and L. J., Zanetti, Large-scale characteristics of magnetospheric equatorial currents, *J. Geophys. Res., 95*, 991, 1990.

Iyemori, T., Storm-time magnetospheric currents inferred from mid-latitude geomagnetic field variations, *J. Geomagn. Geoelectr., 42*, 1249, 1990.

Le, G., and C. T. Russell, Initial Polar magnetic field experiment observations of the low-altitude polar magnetosphere: Monitoring the ring current with polar orbiting spacecraft, *J. Geophys. Res., 103*, 17,345, 1998.

Paularena, K. I., G. N. Zastenker, A. J. Lazarus, and P. A. Dalin, Solar wind plasma correlations between IMP 8, Interball-1, and Wind, *J. Geophys. Res., 103*, 14,601, 1998.

Peredo, M., J. A. Slavin, E. Mazur, and S. A. Curtis, Three-dimensional position and shape of the bow shock and their variation with Alfvenic, sonic, and magnetosonic Mach numbers and interplanetary magnetic field orientation, *J. Geophys. Res., 100*, 7907, 1995.

Russell, C. T., M. Ginskey, and S. M. Petrinec, Sudden impulses at low-latitude stations: Steady state response for northward interplanetary magnetic field, *J. Geophys. Res., 99*, 253, 1994a.

Russell, C. T., M. Ginskey, and S. M. Petrinec, Sudden impulses at low-latitude stations: Steady state response for southward interplanetary magnetic field, *J. Geophys. Res., 99*, 13,403, 1994b.

Sugiura, M., B. G. Ledley, T. L. Skillman, and J. P. Heppner, Magnetospheric field distortions observed by Ogo 3 and 5, *J. Geophys. Res., 76*, 7552, 1971.

Tsyganenko, N. A., Modeling the Earth's magnetospheric magnetic field confined within a realistic magnetopause, *J. Geophys. Res., 100*, 5599, 1995.

Tsyganenko, N. A., Effects of the solar wind conditions on the global magnetospheric configuration as deduced from data-based field models, *Eur. Space Agency Spec. Publ. 389*, 181, 1996.

T. Iyemori, Data Analysis Center for Geomagnetism and Space Magnetism, Faculty of Science, Kyoto University, Kyoto 606, Japan. (iyemori@swdcgw.kugi.kyoto-u.ac.jp)

G. Le and C. T. Russell, Institute of Geophysics and Planetary Physics, University of California, Los Angeles, 6877 Slichter Hall, Los Angeles, CA 90095-1567. (guanle@igpp.ucla.edu; ctrussel@igpp.ucla.edu)

N. A. Tsyganenko, Laboratory for Extraterrestrial Physics, Code 690.2, NASA Goddard Space Flight Center, Greenbelt, MD 20771. (kolya@nssdca.gsfc.nasa.gov)

(Received August 25, 1998; revised November 19, 1998; accepted December 3, 1998.)